Phototocatalytic Lithography of Poly(propylene sulfide) Block Copolymers: Toward High-Throughput Nanolithography for Biomolecular Arraying Applications

ARTICLE *in* LANGMUIR · JANUARY 2009

Impact Factor: 4.46 · DOI: 10.1021/la802727s · Source: PubMed

Phototocatalytic Lithography of Poly(propylene sulfide) Block Copolymers: Toward High-Throughput Nanolithography for Biomolecular Arraying Applications

Jane P. Bearinger,*,† Gary Stone,† Amy L. Hiddessen,† Lawrence C. Dugan,† Ligang Wu,† Philip Hailey,† James W. Conway,‡ Tobias Kuenzler,§ Lydia Feller,§ Simona Cerritelli,|| and Jeffrey A. Hubbell||

Physical and Life Sciences Directorate, Lawrence Livermore National Laboratory L-211, 7000 East Avenue, Livermore, California, Stanford Nanofabrication Facility, Stanford University, Palo Alto, California, Laboratory for Surface Science and Technology (LSST), ETH Hönggerberg, HCI F536, CH-8093 Zurich, Switzerland, and Institute of Bioengineering and Institute of Chemical Sciences and Engineering, Station 15, Ecole Polytechnique Fédérale de Lausanne (EPFL), CH-1015 Lausanne, Switzerland

Received August 20, 2008. Revised Manuscript Received October 22, 2008

Photocatalytic lithography (PCL) is an inexpensive, fast, and robust method of oxidizing surface chemical moieties to produce patterned substrates. This technique has utility in basic biological research as well as various biochip applications. We report on porphyrin-based PCL for patterning poly(propylene sulfide) block copolymer films on gold substrates on the micrometer and submicrometer scales. We confirm chemical patterning with imaging ToF-SIMS and low-voltage SEM. Biomolecular patterning on micrometer and submicrometer scales is demonstrated with proteins, protein-linked beads. and fluorescently labeled proteins.

1. Introduction

Inexpensive, fast, and robust methods of nanomanufacturing represent a grand challenge in nanotechnology. The fabrication of microprocessors, genomic and proteomic assays, crystal growth, and so forth are plagued by problems, including high cost, low throughput and efficiency, and poorly controlled substrate conditions.

Present chemical patterning methodologies applied to biomolecules include photolithography,[1−3] microcontact printing,[4−7] selective molecular assembly patterning (SMAP[8,9]), dip-pen nanolithography,[10−12] colloidal patterning,[13−16] and nanoimprint lithography.[17−19] Nanoscale protein patterning using self-assembled diblock copolymers[20] or pH-reactive polymer films[21] has also been described. (See Christman[22] for a review.) Limitations of these varied techniques include contamination from resists, lack of pattern versatility and resolution, and time and temperature constraints. More recently, photocatalytic lithography employing photocatalytic semiconductors, such as TiO_2, has been demonstrated to overcome many of these limitations.[23−25] However, the reported excitation time is still on the order of minutes, and there are issues with the grain size, material phase, gap spacing above the substrate, and so forth.

New lithographic techniques that significantly reduce the cost and time associated with the fabrication of nanometer-sized features are required. For this purpose, energy from naturally occurring biological materials may be harnessed to induce specific molecular chemical responses. We report on the use of porphyrins, a family of pyrrole-based molecules that may be excited by low-energy, visible wavelength sources to oxidize substrate chemical moieties locally in a matter of seconds, thereby patterning the surface chemistry.

Porphyrin-based photocatalytic lithography[26] works on the time scale of seconds with resolution on the submicrometer scale

* Corresponding author. E-mail: bearinger1@llnl.gov.
† Lawrence Livermore National Laboratory.
‡ Stanford Nanofabrication Facility.
§ Swiss Federal Institute of Technology.
|| Ecole Polytechnique Fédérale de Lausanne.

(1) Thomas, C. H.; Lhoest, J. B.; Castner, D. G.; McFarland, C. D.; Healy, K. E. *J. Biomech. Eng.* **1999**, *121*, 40–48.
(2) Thomas, C. H.; Collier, J. H.; Sfeir, C. S.; Healy, K. E. *Proc. Natl. Acad. Sci. U.S.A.* **2002**, *99*, 1972–1977.
(3) Falconnet, D.; Koenig, A.; Assi, T.; Textor, M. *Adv. Funct. Mater.* **2004**, *14*, 749–756.
(4) Kane, R. S.; Takayama, S.; Ostuni, E.; Ingber, D. E.; Whitesides, G. M. *Biomaterials* **1999**, *20*, 2363–2376.
(5) Jeon, N. L.; Choi, I. S.; Whitesides, G. M.; Kim, N. Y.; Laibinis, P. E.; Harada, Y.; Finnie, K. R.; Girolami, G. S.; Nuzzo, R. G. *Appl. Phys. Lett.* **1999**, *75*, 4201–4203.
(6) Chen, C. S.; Mrksich, M.; Huang, S.; Whitesides, G. M.; Ingber, D. E. *Biotechnol. Prog.* **1998**, *14*, 356–363.
(7) Csucs, G.; Kunzler, T.; Feldman, K.; Robin, F.; Spencer, N. D. *Langmuir* **2003**, *19*, 6104–6109.
(8) Lussi, J. W.; Michel, R.; Reviakine, I.; Falconnet, D.; Goessl, A.; Csucs, G.; Hubbell, J. A.; Textor, M. *Prog. Surf. Sci.* **2004**, *76*, 55–69.
(9) Michel, R.; Lussi, J. W.; Csucs, G.; Reviakine, I.; Danuser, G.; Ketterer, B.; Hubbell, J. A.; Textor, M.; Spencer, N. D. *Langmuir* **2002**, *18*, 3281–3287.
(10) Lee, K. B.; Park, S. J.; Mirkin, C. A.; Smith, J. C.; Mrksich, M. *Science* **2002**, *295*, 1702–1705.
(11) Lim, J. H.; Ginger, D. S.; Lee, K. B.; Heo, J.; Nam, J. M.; Mirkin, C. A. *Angew. Chem., Int. Ed.* **2003**, *42*, 2309–2312.
(12) Lee, K. B.; Lim, J. H.; Mirkin, C. A. *J. Am. Chem. Soc.* **2003**, *125*, 5588–5589.
(13) Fischer, U. C.; Zingsheim, H. P. *J. Vac. Sci. Technol.* **1981**, *19*, 881–885.
(14) Sutherland, D. S.; Broberg, M.; Nygren, H.; Kasemo, B. *Macromol. Biosci.* **2001**, *1*, 270–273.
(15) Andersson, A.-S.; Glasmästar, K.; Hanarp, P.; Seantier, B.; Sutherland, D. S. *Nanotechnology* **2007**, *18*, 205303.
(16) Michel, R.; Reviakine, I.; Sutherland, D.; Fokas, C.; Csucs, G.; Danuser, G.; Spencer, N. D.; Textor, M. *Langmuir* **2002**, *18*, 8580–8586.
(17) Truskett, V. N.; Watts, M. P. C. *Trends Biotechnol.* **2006**, *24*, 312–317.
(18) Falconnet, D.; Pasqui, D.; Park, S.; Eckert, R.; Schift, H.; Gobrecht, J.; Barbucci, R.; Textor, M. *Nano Lett.* **2004**, *4*, 1909–1914.
(19) Zhang, G. M.; Zhang, J; Xie, G. Y.; Liu, Z.F.; Shao, H. B. *Small* **2006**, *2*, 1440–1443.
(20) Kumar, N.; Hahm, J-i. *Langmuir* **2005**, *21*, 6652–6655.
(21) Christman, K. L.; Requa, M. V.; Enriquez-Rios, V. D.; Ward, S. C.; Bradley, K. A.; Turner, K. L.; Maynard, H. D. *Langmuir* **2006**, *22*, 7444–7450.
(22) Christman, K. L.; Enriquez-Rios, V. D.; Maynard, H. D. *Soft Matter* **2006**, *2*, 928–939.
(23) Tatsuma, T.; Kubo, W.; Fujishima, A. *Langmuir* **2002**, *18*, 9632–9634.
(24) Kubo, W.; Tatsuma, T.; Fujishima, A.; Kobayashi, H. *J. Phys. Chem. B* **2004**, *108*, 3005–3009.
(25) Lee, J. P.; Sung, M. M. *J. Am. Chem. Soc.* **2004**, *126*, 28–29.

10.1021/la802727s CCC: $40.75
Published on Web 12/29/2008

and without many of the limitations of photocatalytic semiconductor-based lithography. A photocatalyst is bound to the surface of a patterned stamp mask and is in contact with an appropriately sensitive organic adlayer for patterning on a substrate. The stamp is a mask not in the sense of blocking light exposure to certain regions but rather in the sense of localizing chemical reactivity to the areas of the contact between the stamp and the adlayer. In contrast to usual stamping, mass is not transferred from the stamp to the substrate; as such, we refer to it as a mask. It is advantageous that photocatalytic lithography may achieve feature resolution smaller than the wavelength of excitation. It is not substrate- or surface-chemistry-dependent, and it quickly and inexpensively chemically patterns substrates on the micrometer and submicrometer scales.

In this work, we employ poly(propylene sulfide)-*bl*-poly(ethylene glycol) (PPS-PEG), block copolymers, to passivate gold surfaces. Poly(propylene sulfide) (PPS) chemistry and derivatives thereof were first described as oxidation-sensitive polymersomes.[27] PPS polymers chemisorb stably with gold via the sulfur atom in the sulfide moiety[28] and have shown efficacy toward passivating surfaces.[28,29] In colloidal forms, PPS-PEG copolymers have been explored in drug delivery[30−32] as well as in lymph nodes in vaccination[33] and in binding after functionalization in cartilage.[34]

We photocatalytically pattern PPS-PEG on the micrometer and submicrometer scales to realize microarray-formatted gold surfaces as well as irregularly patterned surfaces with varying feature aspect ratios. Because the chemisorption of the polymer to gold is mediated by the sulfur atom in the sulfide and the sulfide is particularly sensitive to reaction with the photocatalytically generated reactive oxygen species, PPS-PEG is a particularly interesting polymer in photocatalytic lithography. We characterize the patterned surfaces with optical microscopy, time-of-flight secondary ion mass spectrometry (ToF-SIMS), and low-voltage scanning electron microscopy (LV SEM), and we demonstrate selective protein patterning via atomic force microscopy, protein-conjugated beads, and fluorescence microscopy.

2. Experimental Section

2.1. Substrates. Substrates of gold evaporated on silicon wafers (Platypus Technologies, Madison, WI) were used in all experiments. Substrates were typically scribed (or cut with a diamond-tipped scribe) to approximately 1 cm^2 areas, cleaned by sonicating in ethanol for a few minutes, blown dry in a stream of nitrogen, and then exposed to UV ozone (Jelight 144AX, Irvine, CA) for 1 min.

2.2. Mask Masters. Masters for the micrometer-scale structures were produced as described in a prior publication, using silicon wafers and traditional photolithography.[26] The masters contained patterns of variously sized circular spot regions, separated by a distance equivalent to their diameters or square-within-square regions with a 5 μm pitch (Figure 2).

The masters for the nanometer-scale structures were fabricated by electron-beam lithography (EBL) using a Raith150 system (Raith GmbH, Dortmund, Germany).

After being cleaned, the silicon masters were coated with 264-nm-thick ZEP-520 positive tone electron beam resist (ZEON Corp., Tokyo Japan) and soft baked for 120 s at 200 °C. The resist was then exposed to an electron beam at an acceleration voltage of 20 kV using an electron dose of 70 $\mu C/cm^2$ for all patterns. The beam current measured 0.146 nA. After EBL exposure, the resist was developed in xylenes for 40 s with gentle agitation, soaked in a methyl isobutyl ketone/ isopropyl alcohol (MIBK/IPA) 1:3 solution for 30 s at 22 °C, and then rinsed with pure 2-propanol for 30 s.

After lithography, the samples were reactively ion etched (RIE) in an Applied Materials P-5000 MERIE system in a two-step RIE process. The initial breakthrough step removed the intrinsic native silicon dioxide layer over the silicon substrate using CF4 for 5 s (100 mT, 250 W), followed by RIE of the silicon substrate using a 1:1 ratio of Cl_2 to HBr for 1 min (100 mT, 250 W 40 G magnetic field). The ZEP-520 thin film was stripped using Piranha etchant (9:1 H_2SO_4/ H_2O_2, 120 °C.)

2.3. Photomask Fabrication. Micrometer-scale masks were constructed from masters using PDMS (Sylgard 184, Dow Corning, Midland, MI).[26] Affinity polyolefin plastomers (POP)[7] were used to construct nanoscale masks. These materials are copolymers of ethylene and R-olefin (butane or octane) and undergo metallocene polymerization, which selectively polymerizes the ethylene and comonomer sequences. POP pellets (Affinity EG8200, Dow Chemical Company, Midland, MI) were melted into blocks of 40 × 20 × 5 mm^3 at 190 °C under a pressure of 4 bar using an appropriate metal template. Thin polyimide foils were placed between metal and melted polymer to avoid sticking. After cooling to room temperature (RT), the solid polymer bars were removed from the template, rinsed with ethanol, and dried in a stream of nitrogen. In the next step, the bars were placed over the masters (10 × 10 mm^2) and placed between two silicon wafers. This "sandwich" was then placed on a hot plate (heated to 130 °C from both sides). A weight of 200 g was put on the top of the sandwich for 5 min, followed by a weight of 700 g for 4 min. After cooling, the master was peeled away from the POP bar, which was then cut to its proper size with a razor blade. Prior to use, the POP masks were cleaned with acetone for 5 min in an ultrasonic bath.

2.4. PPS-PEG Synthesis and Surface Passivation. As previously described,[29,35] symmetric triblock poly(propylene sulfide)-*block*-poly(ethylene glycol) copolymers with a PPS backbone of 3.9 kDa and two PEG end chains of 2 kDa were synthesized by a one-pot process. The PPS-PEG block copolymer was ultrasonically dissolved in methanol at a concentration of 1 mg/mL. Gold substrates were immersed in the solution for approximately 30 min and then ultrasonically cleaned in methanol for a few seconds to remove multilayered, loosely bound material. Substrates were dried in a stream of nitrogen prior to patterning.

2.5. Photocatalytic Patterning. We used magnesium phthalocyanine (MgPC, Sigma-Aldrich, St. Louis, MO), hematoporphyrin(IX) dihydrochloride (HP, Frontier Scientific, Logan, UT), or chlorophyllin sodium copper salt (Chlor, Sigma-Aldrich) as the patterning photocatalyst. A cotton swab dipped in solvated porphyrin (in ethanol (Sigma-Aldrich, St. Louis, MO), 1 mg/mL) was used to coat PDMS- or POP-based photomasks. The porphyrin-coated masks were blown dry with nitrogen. We also explored placing a drop of solution on masks and then blowing off the excess material after 5 s with a light blast of nitrogen. This was done to preclude damage to the masks with coarse fibers from the cotton swabs, which sometimes resulted in scratches.

Masks were placed by hand on top of PPS-PEG-coated Au. Controlled patterning and removal of the PPS-PEG was achieved by local oxidation via approximately 5 s of activation of the photocatalyst through the polymeric photomask with 660 nm red LED light (Lumex, Glenview, IL; or Superbright LEDs, St. Louis,

(26) Bearinger, J. S.G; Christian, A. T.; Dugan, L; Hiddessen, A. L.; Wu, K. J.; Wu, L; Hamilton, J; Stockton, C; Hubbell, J. A. *Langmuir* **2008**, *24*, 5179–5184.
(27) Napoli, A.; Valentini, M.; Tirelli, N.; Muller, M.; Hubbell, J. A. *Nat. Mater.* **2004**, *3*, 183–189.
(28) Bearinger, J. P.; Terrettaz, S.; Michel, R.; Tirelli, N.; Vogel, H.; Textor, M.; Hubbell, J. A. *Nat. Mater.* **2003**, *2*, 259–264.
(29) Feller, L. M.; Cerritelli, S.; Textor, M.; Hubbell, J. A.; Tosatti, S. G. P. *Macromolecules* **2005**, *38*, 10503–10510.
(30) Velluto, D.; Demurtas, D.; Hubbell, J. A. *Mol. Pharm.* **2008**, 632–642.
(31) Cerritelli, S.; Velluto, D.; Hubbell, J. A. *Biomacromolecules* **2007**, *8*, 1966–1972.
(32) Segura, T.; Hubbell, J. A. *Bioconjugate Chem.* **2007**, *18*, 736–745.
(33) Reddy, S. T.; Rehor, A.; Schmoekel, H. G.; Hubbell, J. A.; Swartz, M. A. *J. Controlled Release* **2006**, *112*, 26–34.
(34) Rothenfluh, D. A.; Bermudez, H.; O'Neil, C. P.; Hubbell, J. A. *Nat. Mater.* **2008**, *7*, 248–254.
(35) Napoli, A.; Tirelli, N.; Kilcher, G.; Hubbell, J. A. *Macromolecules* **2001**, *34*, 8913–8917.

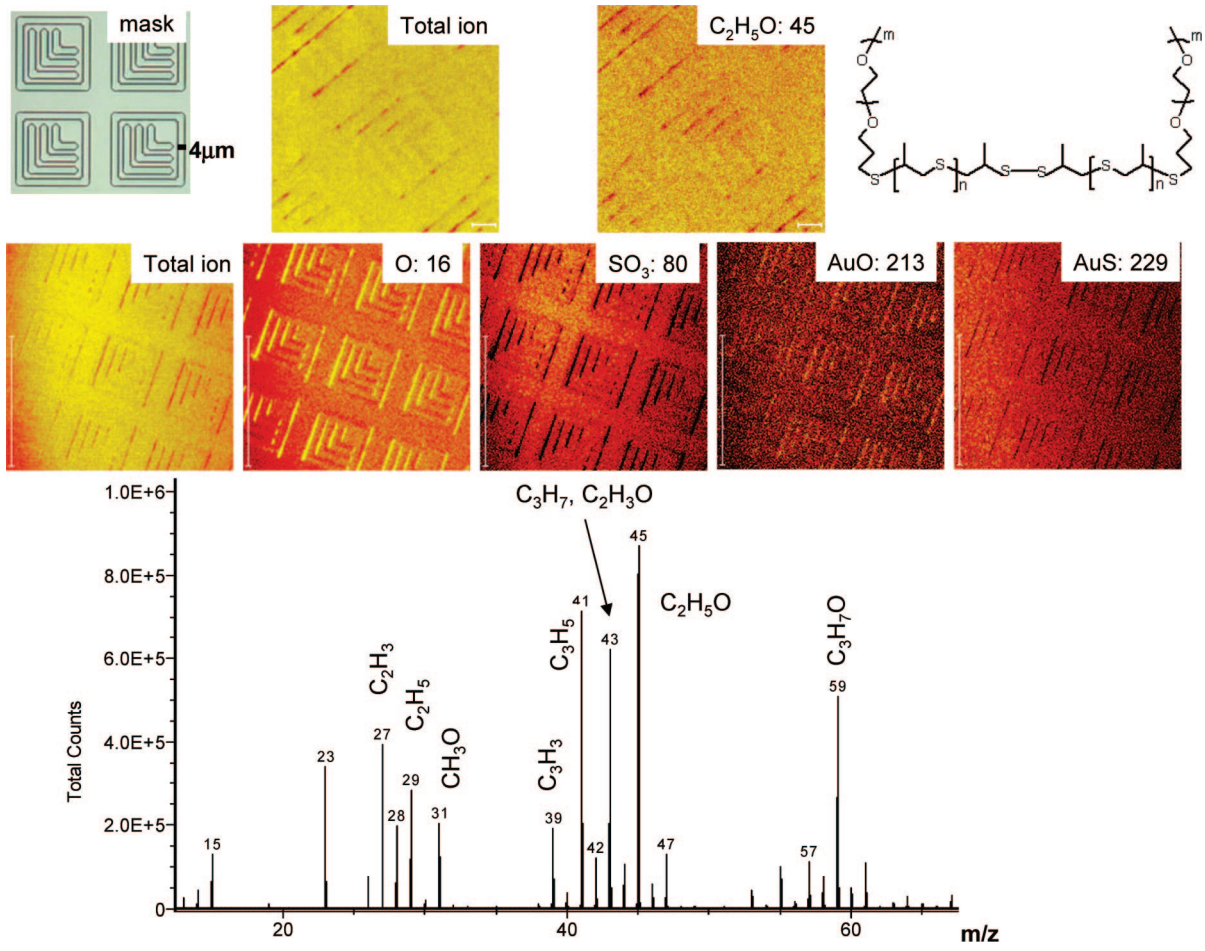

Figure 1. ToF-SIMS imaging: positive-mode (top row, scale bar = 10 μm) and negative-mode (bottom row, scale bar = 100 μm) results for photocatalytically patterned PPS-PEG on Au. (MgPC is used as a photocatalyst, and PDMS is used as a mask). The matrix is enriched with fragments representing PEG hydrocarbons, oxygen species linked to gold and sulfur, and gold−sulfur species. Patterned features exhibited reduced counts; however, hydrogen enrichment was noted. The bottom spectral analysis window from positive imaging indicates significant quantities of hydrocarbon and PEG moieties (*m*/*z* ratios plotted).

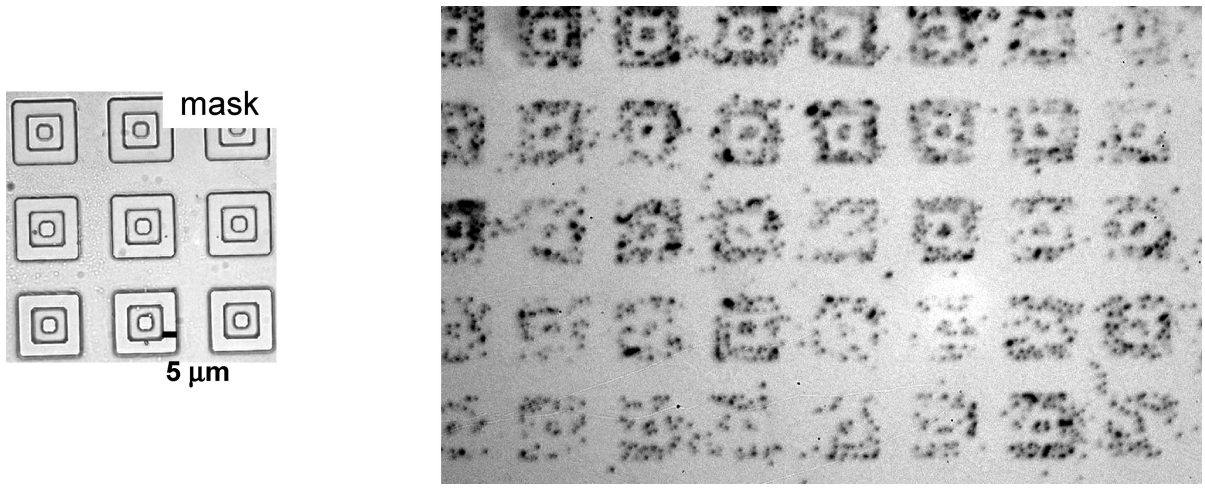

Figure 2. Fibronectin-linked beads adsorbed onto a PPS-PEG/Au patterned surface. (HP was used as photocatalyst, and PDMS was used as a mask.) Protein adsorbs onto gold regions where PPS-PEG was photocatalytically removed. PPS-PEG retained on the matrix repels protein adsorption. The central square diameter and outer square line width are each 5 μm.

MO). Localized patterning and oxidation of PPS-PEG occurred at locations on the raised portions of the photomask in close contact with the coated gold. PPS-PEG regions positioned under the recessed photomask remained uncompromised. Patterned surfaces were sonicated in solvent for approximately 10 s and blown dry with nitrogen. Control experiments were performed via exposure of PPS-PEG-coated substrates to photomasks without porphyrin in the presence of excitation energy (light).

2.6. Methods of Analysis. *2.6.1. Time-of-Flight Secondary Ion Mass Spectometry (ToF-SIMS).* Time-of-flight secondary ion mass spectometry (ToF-SIMS) measurements were conducted on a PHI-TRIFT III instrument (Physical Electronics USA; Chanhassen, MN)

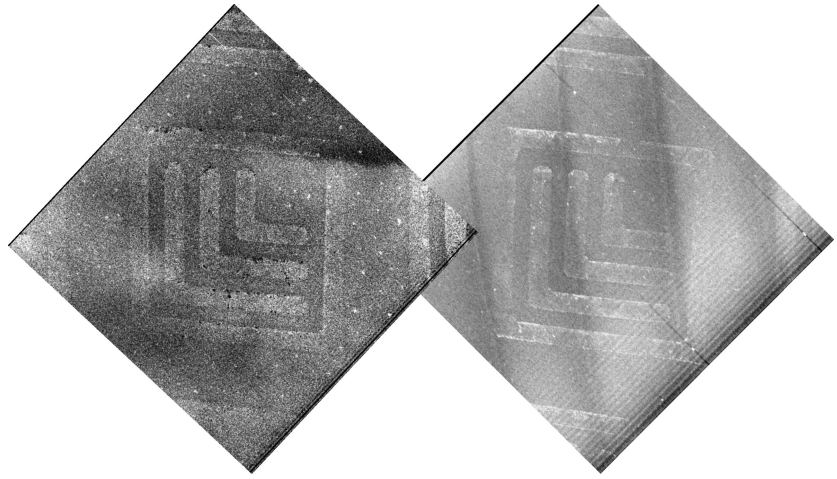

Figure 3. Fibronectin adsorbed onto a PPS-PEG/Au patterned surface. (HP was used as a photocatalyst, and PDMS was used as a mask.) Friction- (left) and height-mode (right) AFM, line width = 4 μm, and scan width = 75 μm. Results indicate that fibronectin adsorbs onto gold regions that underwent photocatalytic removal of nonfouling PPS-PEG polymer (L boxes).

equipped with a gallium liquid metal ion gun (Ga LMIG). The ion gun was operated at either 25 kV (unbunched mode) for high image resolution or 15 kV (bunched mode) for high mass resolution. Analyses were done by utilizing Ga^+ at RT. ToF-SIMS measurements were conducted over a 100 × 100 μm^2 area for 10 min in positive mode and over a 175 × 175 μm^2 area for 10 min in negative mode. The positive mass spectra were calibrated using common hydrocarbon fragment peaks at CH_3^+, $C_2H_3^+$, and $C_4H_7^+$, and the negative mass spectra were calibrated using CH^-, OH^-, and C_2H^-. Spectra for background controls were acquired by analyzing clean gold areas on the wafers.

2.6.2. Scanning Electron Microscopy (SEM). A Quanta 200 environmental scanning electron microscope was used in high-vacuum mode. Imaging of substrates was performed using the secondary electron detector at 1 kV and a spot size of approximately 100 nm. No staining was necessary to image patterned polymer films.

2.6.3. Atomic Force Microscopy (AFM). Features on patterned gold substrates were imaged using a Digital Instruments Dimension 3100 atomic force microscope (Digital Instruments/Veeco Metrology Group, Inc.; Santa Barbara, CA) with SiN (DNP-S) probes. Contact-based friction and topographic modes were utilized.

2.7. Protein Adsorption Experiments. *2.7.1. Preparation of Protein-Linked Beads.* Streptavidin-coated, 0.9-μm-diameter latex beads (Bangs Laboratories, Inc.; Fishers, IN) were incubated in a solution of 40 μg/mL biotinylated antifibronectin antibody (rabbit IgG) (Rockland Immunochemicals, Inc.; Gilbertsville, PA) within phosphate-buffered saline containing 1% bovine serum albumin (w/v in PBS) for 1 h at RT. The antifibronectin conjugated beads were then washed five times in PBS/BSA (1%) solution and finally resuspended in PBS solution for use in protein adsorption experiments.

2.7.2. Protein Adsorption. Protein-linked bead experiments were carried out on photocatalytically patterned PPS-PEG/Au substrates by first immersing the substrates in phosphate-buffered saline (PBS, pH, 7.4) for about 1 min and then immersing the substrates in a 0.5 mg/mL fibronectin (Gibco) in PBS solution for 1 h. Substrates were then washed three times in PBS and immersed in a solution of 0.9 μm antifibronectin conjugated beads for approximately 2 h. Finally, the substrates were rinsed in deionized (DI) water and air dried. Imaging was performed using a Nikon D100 camera mounted on a reflectance-based Nikon Labophot 2 microscope. Fibronectin adsorption in the absence of conjugated beads was characterized using AFM. Substrates were imaged in contact mode by friction and height.

Fluorescently labeled protein experiments were conducted by first immersing photocatalytically patterned PPS-PEG on Au substrates in a 25 μg/mL solution of recombinant protein A (Pierce Biotechnologies; Rockford, IL) in PBS for approximately 1 h at RT. After thoroughly rinsing in PBS, the substrates were then immersed in 20 μg/mL fluorescein isothiocyanate IgG (FITC-IgG, Santa Cruz Biotechnology, Inc.; Santa Cruz, CA) in PBS for 30 min. The detection of FITC-labeled IgG on surfaces exposed to fluorescent proteins was performed using a Zeiss Axiovert 200 M materials microscope equipped with a dark field, epifluorescence, an FITC filter set, and a Zeiss Axiocam HRM high-resolution digital camera. Images were captured using Zeiss Axiovision software.

3. Results and Discussion

We demonstrate PPS-PEG patterning on the micrometer and submicrometer scales using porphyrin-based photocatalytic lithography. We exploited the nonfouling surface passivation capabilities of PPS-PEG to pattern biomolecules selectively on regions of the surface where PPS-PEG had been photocatalytically removed to reveal bare gold regions. In contrast to microcontact printing, this patterning technique allows for the formation of pinhole-free films because the films completely cover the substrate prior to patterning by selective removal of the polymer adlayer. Because the purpose of the mask is to localize the chemical reactivity at points of contact with the adlayer on the substrate rather than to transfer mass from a stamp to the substrate, many of the irregularities of films transferred from a stamp by physical forces can be avoided. Furthermore, because the adlayer that is the final desired surface chemical functionality is also the resist, the process is potentially cleaner than when traditional photolithographic resists are used and then replaced positively or negatively with the desired final adlayer.

3.1. Chemical Patterning Demonstrated by ToF-SIMS and AFM. One of the best ways of confirming chemical patterning is using imaging ToF-SIMS. It is relatively nondestructive and extremely surface-sensitive. Our ToF-SIMS results (Figure 1) from positive and negative ion mode imaging indicate the presence of PPS-PEG on the gold substrates and the absence of PPS-PEG from photocatalytically patterned regions. ToF-SIMS analysis of larger patterns generated by photocatalytic means supports the complete removal of PPS-PEG (data not shown).

Combining results from positive and negative mode imaging and accompanying spectral analysis windows, we see that the matrix is enriched with the cracking patterns that one would expect from PEG after exposure to the Ga^+ beam, including oxygen species linked to gold and sulfur and gold−sulfur species. Patterned features (Ls in this case) typically had reduced mass/

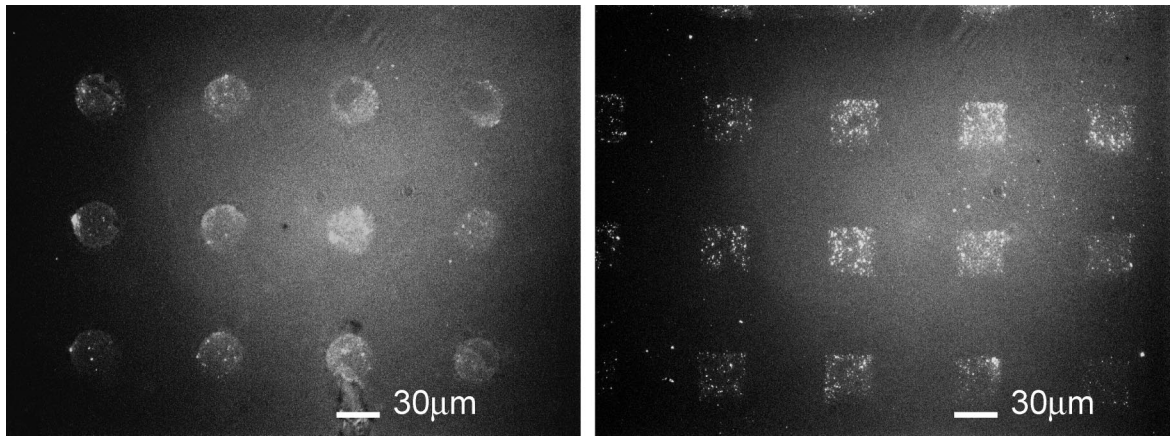

Figure 4. Adsorption of A/FITC IgG protein on PPS-PEG photocatalytically patterned on Au. (Chlor was used as a photocatalyst, and PDMS was used as a mask. Each scale bar = 30 μm.)

charge (m/z) ratios; thus, it was difficult to image fragments of higher intensity on patterned feature regions. However, hydrogen enrichment was noted on some patterned features.

It is clear that the contrast in the positive ion, the PEG fragment ($m/z = 45$) image, is of lower contrast than some of the negative ion images. The ion yield of PEG positive ion fragments is relatively low, and the resultant image contrast is therefore inferior because of the poor signal/noise ratio. In contrast, ToF-SIMS is very sensitive to metals and oxides because they are easily ionized. Thus, in negative mode, the ion yield of O ($m/z = 16$) and SO_3 ($m/z = 80$) is high, and the images indicate improved contrast. The addition of gold ions, AuO ($m/z = 213$) and AuS ($m/z = 229$), indicated moderate contrast because they are high-mass ions. Higher-mass ions tend to produce lower counts because they have an associated longer flight time in the mass spectrometer and thus a higher chance of breaking down.

It should be noted that micrometer-scale patterning was obtained using PDMS as the photomask material and this did present surface contamination on a few of the samples examined. The advantageous material properties of PDMS are its inherent transparency to radiation at the wavelengths employed and its ability to act as a lens material.[36−38] Furthermore, it is reusable and contains large amounts of oxygen to facilitate radical formation. For submicrometer-scale patterning, we utilized POP,[7] a polyolefin elastomer from Dow, as our photomask material of choice. POP maintains good transparency to the wavelengths of light employed and has superior mechanical properties for our purposes, such as a higher modulus as compared to that of PDMS.

We also note that AFM measurements indicate that 1 μm^2 rms roughness measurements of PPS-PEG on gold and on gold regions where PPS-PEG had been removed were not significantly different, although the value for PPS-PEG on gold was lower than on the gold itself: 1.6 versus 1.8. This result follows the same trend observed with the PPS-PEG coating lowering the bare gold roughness rms before PPS-PEG application. The height difference of the PPS-PEG layer was measured by AFM to be 3.2 nm, similar to the results from Feller et al. of 3.4 nm by ellipsometry.[29]

3.2. Protein Adsorption onto Lithographically Dictated Regions. Figures 2−4 show micrometer-scale patterning of protein adsorption on PPS-PEG-coated gold surfaces subjected to photocatalytic patterning. Fibronectin-linked beads adsorbed onto a PPS-PEG/Au patterned surface are shown in Figure 2. PPS-PEG retained on the gold substrate repels protein adsorption, whereas protein-linked beads aggregate onto the exposed gold regions at sites where PPS-PEG was photocatalytically removed.

Figure 3 shows micrometer-scale AFM results of fibronectin adsorbed onto a PPS-PEG/Au patterned surface. Height and friction contact-mode imaging indicate fibronectin adsorption onto gold regions where PPS-PEG had been photocatalytically removed. In Figure 4, we show a sequential protein-labeling approach for the first adsorbing protein A onto patterned surfaces, rinsing, and then adsorbing FITC-labeled IgG on surfaces. This two-step, linked approach was used for optical visualization because (a) it gives further credence to the passivating properties of PPS-PEG (repeated protein exposure) and (b) gold quenches fluorescence within the Förster distance of its surface, whereas the tethering of two proteins extends the structure beyond this distance and fluorescence is visualized.

3.3. Nanoscale Pattern Imaging and Protein Adsorption. Submicrometer (large nanoscale) patterning performed with a POP mask is seen in Figure 5. Low-voltage SEM was used to characterize PPS-PEG photocatalytically patterned on gold. The low-voltage SEM image indicates more secondary electron transmission from gold regions where PPS-PEG was removed, as compared to the PPS-PEG matrix that acts as an insulator. In other words, the contrast in the SEM is due to the differential way in which electrons interact with the polymer film (insulator) versus the gold substrate (conductor). Similar properties have been described on silicon backgrounds and with block copolymers.[39−41] The regions where PPS-PEG has been removed therefore appear to be brighter because of the greater secondary electron signal from gold.

After we confirmed the ability to pattern on the submicrometer scale, we again challenged our surfaces to biomolecular adsorption. Figure 6 shows tethered protein (protein A and FITC-IgG) adsorbed onto patterned gold regions and the absence of protein on PPS-PEG matrix regions. The top left of the image indicates a receding solvent front of fluorescent proteins in solution to describe the passivating properties of PPS-PEG more dynamically.

3.4. Utility and Estimated Resolution Limits. Because such small quantities of gold are now necessary to realize sensor

(36) Camou, S.; Fujita, H.; Fujii, T. *Lab Chip* **2003**, *3*, 40–45.
(37) Chen, J.; Wang, W. S.; Fang, J.; Varahramyan, K. *J. Micromech. Microeng.* **2004**, *14*, 675–680.
(38) Agarwall, M.; Gunasekaran, R. A.; Coane, P.; Varahramyan, K. *J. Micromech. Microeng.* **2004**, *14*, 1665–1673.
(39) Harrison, C.; Park, M.; Chaikin, P. M.; Register, R. A.; Adamson, D. H. *J. Vac. Sci. Technol., B* **1998**, *16*, 544–552.
(40) Gaillard, C.; Stadelmann, P. A.; Plummer, C. J. G.; Fuchs, G. *Scanning* **2004**, *26*, 122–130.
(41) Drummy, L. F.; Yang, J. Y.; Martin, D. C. *Ultramicroscopy* **2004**, *99*, 247–256.

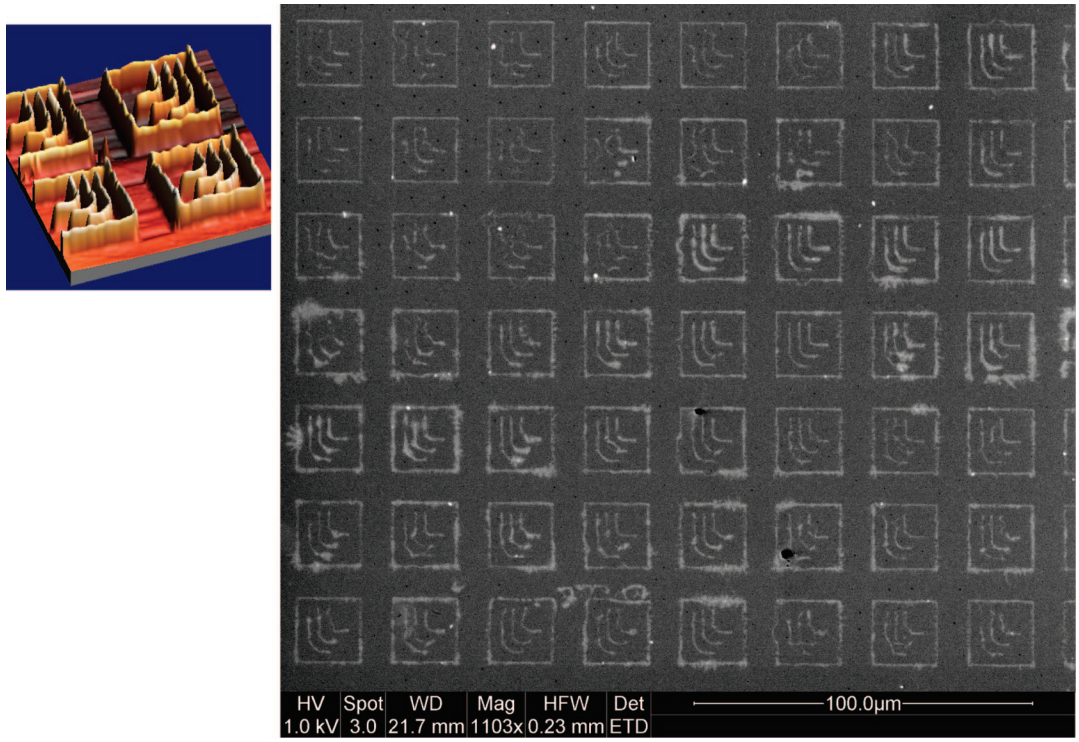

Figure 5. Low-voltage SEM used to characterize PPS-PEG photocatalytically patterned on Au. (MgPC is used as a photocatalyst.) Regions where PPS-PEG was removed appear to be brighter (Ls, line width = 600 nm) because of the greater secondary electron signal from gold. PPS-PEG acts as an insulator. The inset shows an AFM surface plot of the POP mask: 20-μm-wide features, 600 nm line width, and ~300 nm height.

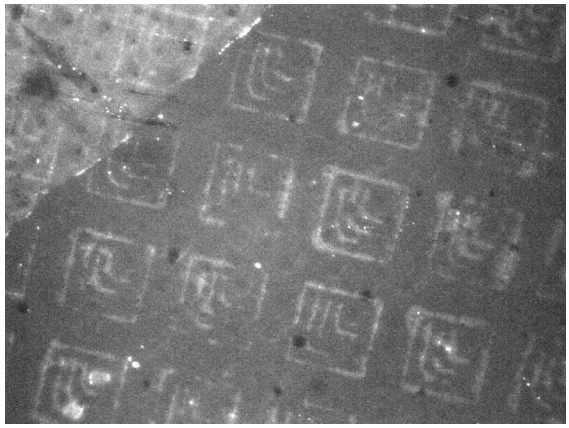

Figure 6. Fluorescence microscopy was used to characterize PPS-PEG photocatalytically patterned on Au. (MgPC was used as a photocatalyst, and POP was used as a mask.) Acquisition magnification is 100×. Fluorescent protein adsorbs where PPS-PEG was removed (Ls, line width = 600 nm); protein is repelled from the remaining PPS-PEG-coated regions. The top left corner shows the receding solvent front of fluorescent protein in solution.

surfaces and basic scientific research seeks to arrange nanoscale ligands selectively in a dictated fashion, photocatalytic patterning of PPS-PEG on gold holds promise as a novel methodology for adoption by industry and academia alike. Stable, protein-repulsive PPS-PEG adlayers can be formed on gold, and these adlayers can be selectively removed to expose the underlying gold via photocatalytic lithography. The technique avoids the wavelength-dependent pitfalls of traditional photolithography and, unlike stamping, avoids the complexities of the transfer of materials from one object to another.

To estimate the actual resolution limits of this technique, we first compare photocatalytic semiconductors to porphyrin-based activity. Photocatalytic semiconductors rely on generating electron−hole pairs that subsequently generate radical oxygen species after escaping from the source particle and interacting with oxygen. Electron−hole pairs generated in TiO_2 may migrate ~75 nm from their source in a free field region.[42,43] In general, the ability to guarantee electron−hole pair escapes can be influenced by the intensity of input energy (i.e., light).

In contrast to photocatalytic semiconductors such as TiO_2, which have been reported to be patterning photocatalysts,[23,24] excited photosensitizers such as porphyrins generate radical oxygen species (ROS) directly, thereby mitigating concerns about electron−hole pair diffusion. However, the diffusion of radical oxygen species, including electron-generated singlet oxygen and hole-generated hydroxyl radicals, may also be expected to limit resolution. As more fully described in an initial publication,[26] it is estimated that the distance diffused by singlet oxygen is on the order of 10−20 nm, corresponding to a lifetime of 10−40 nS,[44] whereas the distance diffused by hydroxyl radicals in C−H environments is about 4 nm.[45] When exposed to a polymer adlayer positioned on a substrate, the reactive species likely oxidize the adlayer and thus are consumed within a few nanometers of their origin. We estimated the feasibility of feature generation as small as 50 nm, assuming that proper mechanics are devised to position porphyrin-bearing photomasks on surfaces appropriately and assuming sufficiently constrained species migration (i.e., atmospheric conditions).

However, we have not yet realized this theoretical limit and presently have achieved resolution on the order of 200 nm on substrates that may include pinholes and/or contaminants (Figures 2−4). The issues that presently preclude us from reaching 50 nm

(42) Gautron, J.; Lemasson, P.; Marucco, J. F. *Faraday Discuss.* **1980**, 81–91.
(43) Carp, O.; Huisman, C. L.; Reller, A. *Prog. Solid State Chem.* **2004**, *32*, 33–177.
(44) Moan, J. *Photochem. Photobiol.* **1986**, *43*, 681–688.
(45) Moan, J.; Berg, K. *Photochem. Photobiol.* **1991**, *53*, 549–553.

resolution are photosensitizer solubility, mask design and implementation, and polymer molecular weight.

The studies herein included the use of magnesium phthalocyanine, hematoporphyrin(IX) dihydrochloride, or chlorophyllin sodium copper salt in ethanol. Phthalocyanine analysis in solution has been hindered by its limited solubility in many solvents. Among the four-coordinate metal(II) phthalocyaninato complexes, magnesium phthalocyanine exhibits the highest solubility.[46] Solubility is high in solvents such as DMF and acetone; methanol has been used for recrystallization purposes.[47] Hematoporphyrin(IX) dihydrochloride and chorophyllin salts are water-soluble.

Our technique to date delivers photosensitizer to masks via a volatile solvent. As such, water is not volatile enough to enable practical use in our coating mechanism, and the use of most organic solvents has deleterious physical affects on our elastomeric masks. We therefore compromised solubility parameters for technique speed and used ethanol as a volatile solvent that showed acceptable, but not perfect, molecular solvation.

We believe that the presence of pinhole defects and contaminants that can be seen in the Figures results from the aggregation of imperfectly solvated photosensitizer, resulting in PPS-PEG removal in some matrix regions where PPS-PEG was first applied as an intact layer. In essence, photosensitizer contacted the substrate surface where it was not intended and resulted in the photocatalytic removal of PPS-PEG. This result is more prevalent on substrates exposed to protein solution than on substrates composed only of PPS-PEG and gold (Figure 5).

Mask designs were based on the use of PDMS for micrometer-scale patterns and POP for submicrometer patterns. As reported earlier via ToF-SIMS, PDMS may lead to substrate contamination.[26] We believe that this may contribute to the lack of homogeneity present in Figure 4. To date, we as well as collaborative groups have improved our success in terms of increased mechanical properties and decreased surface contamination with POP. However, the AFM inset in Figure 5 indicates a very slight wall height ripple. Whereas the low-voltage SEM in Figure 5 indicates a relatively complete patterning result, Figure 6 indicates a less than perfect feature map of adsorbed biomolecules that may result from this imperfect wall height. Additionally, all masks were placed by hand onto substrates for photocatalytic treatment. No force was applied to masks during the application of light. Future studies should investigate whether the application of mild, evenly applied force eliminates this imperfect result.

The PPS-PEG molecular weight was approximately 8K, with PEG chains coiled above the PPS layer adsorbed on gold. The SEM result shown in Figure 5 suggests some line feature blurring or bleeding. We hypothesize that this is due to the high molecular diffusion of both the activated oxygen moving through the liquid PPS-PEG layer and the potential diffusion of the PPS-PEG itself. To date, we have obtained superior results by photocatalytically patterning silane chemistries on silicon (line widths of 200 nm; results in a forthcoming publication) rather than by patterning the liquid layers of PPS-PEG on gold (line widths of 600 nm as in Figures 5 and 6). We hypothesize that patterning smaller PPS-PEG chemistries, such as PEG_{17}-*bl*-PPS_{25}-*bl*-PEG_9[28] will result in increased resolution. Also, we believe that reducing the substrate temperature will assist in improving patterning resolution using PPS-PEG-type chemistries, but we have not investigated the temperature range in which molecular diffusion is impeded and molecular crystallization is avoided.

4. Conclusions

Porphyrin-based photocatalytic lithography was used to pattern PPS-PEG films on gold substrates on the micrometer and submicrometer scales. Imaging ToF-SIMS and low-voltage SEM confirmed the chemical patterning and quality of the films. Protein adsorption and derivative techniques were used to document high-fidelity biomolecular patterning on a nonfouling background. This method represents an inexpensive, fast, and robust method of oxidizing surface adlayers in order to produce patterned substrates. We believe that this technique can impact basic biological research as well as various biochip applications.

Acknowledgment. We gratefully acknowledge funding from NIH R21 EB003991. This work was partially performed under the auspices of the U.S. Department of Energy at Lawrence Livermore National Laboratory under contracts W-7405-Eng-48 and DE-AC52-07NA27344. We also greatly appreciate Nancy Latta's RIE efforts as well as John Reynolds', Tom Wilson's, and Ken Michlitsch's contributions.

LA802727S

(46) Kasuga, K.; Tsutsuo, M. *Coord. Chem. Rev.* **1980**, *32*, 67–95.
(47) Van Keuren, E.; Bone, A.; Ma, C. *Langmuir* **2008**, *24*, 6079–6084.